AEROBALLISTICS RANGE TESTS OF THE CF-105

PHASE 2 -- MODELS 10-11 TO 10-25

by

H.R. Warren & B. Cheers

DEFENCE RESEARCH BOARD

CANADIAN ARMAMENT RESEARCH AND DEVELOPMENT ESTABLISHMENT

Valcartier, Quebec

November, 1959

NOTE

CARDE Technical Memoranda are prepared for the purpose of distributing information on technical subjects or interim reporting on unfinished projects. They may contain information which is tentative.

CARDE TECHNICAL MEMORANDUM AB-46

PCC NO. D44-03-01-04

CONFIDENTIAL

AEROBALLISTICS RANGE TESTS OF THE CF-105

PHASE 2 -- MODELS 10-11 TO 10-25

by

H.R. Warren*
and
B. Cheers

* The de Havilland Aircraft of Canada, Limited

CANADIAN ARMAMENT RESEARCH AND DEVELOPMENT ESTABLISHMENT

VALCARTIER, P.Q. MARCH 31, 1959

CONTENTS

LIST OF FIGURES

1.0 INTRODUCTION

The first phase of the CF-105 program of tests in the aeroballistics range was described in Ref. 1. It was noted that Phase 1 was largely exploratory -- its purpose being to establish manufacturing and metrology methods, to develop special adaptations of the launching and card-reading methods as applied to aircraft and to develop methods of analysing the test records to derive the aircraft's stability and performance parameters. In the second phase of the program, using models representing the latest configuration of the aircraft, the range of launch speeds was increased to a Mach number of 2.5 in order to obtain dynamic stability data at speeds beyond those of any previous tests on the aircraft. Although this was the original purpose of the Phase 2 tests - to obtain useful information rather than to develop a method - a useful extension of the method is suggested by the study of aeroelastic effects on the stability of aircraft at high speeds.

All the Phase 1 models were launched at M = 1.6 and except for four rounds which were unsuccessful because of either structural defects (Nos. 2, 6 and 7) or unsatisfactory range instrumentation (No. 1), the flights were stable and produced aerodynamic derivative values in good agreement with those obtained using other test methods. With the Phase 2 models, there were again structural difficulties associated with launching as the test Mach number was increased, resulting in the loss of two models. In addition to this however, a form of instability developed at higher speeds which affected four models and which made it impossible to apply the method of analysis developed in Refs. 1 and 2. Assistance was received from Avro Aircraft, Ltd., in analysing these rounds, so that the cause of the instability was determined, as reported herein.

From the total of 15 models, therefore, there were 2 which were lost because of an unsuccessful launch, 4 which were unstable and gave some useful aerodynamic information while the remaining 9 were stable and produced specific values for the stability derivatives.

2.0 TEST METHODS

The methods of model manufacture and metrology and the techniques for launching the models and reading yaw card cuts are essentially the same as those given in Refs. 1 and 2. In the following sections, therefore, only the improvements made specifically for the Phase 2 models will be described.

2.1 Methods of Manufacture

The view of the Phase 2 model in Figure 1 shows the alterations to the nose and aft fuselage which were made to bring the geometry up to date with that of the Mark II CF-105 (cf. Figs. 2 and 3 of Ref. 1). To produce these models, the new masters shown in Figure 2 were prepared. These were copies, using the Pantograph Die-Sinker milling machine, from a 1/80th scale high-speed wind tunnel model loaned by the National Aeronautical Establishment. Before making this copy, the accuracy of profile of the wind tunnel model was checked against the

figures given in Ref. 3 by fixing the model to the bed of a jig bore machine and taking height and thickness measurements at a large number of reference points on the wings and fuselage.

Because a variety of elevator deflections were required to trim the models over the wide range of Mach numbers of the tests, several sets of interchangeable elevator inserts were made for the masters so that each model would have an elevator deflection appropriate to its launch Mach number. Other details of construction of the models are shown in the three-view drawing of Figure 3.

A new template jig was prepared as shown in Figure 4 to check the wing profiles and fuselage sections during manufacture, and as a final check of the profiles before the models were launched, measurements were taken along several wing-chord lines of the wing thickness and height of the upper profile above datum using the method described in Ref. 2. Error plots were then prepared of the difference between the measured profiles and those given in Ref. 3. In cases where the error exceeded $\pm$ .005", the models were reworked.

For the tests at higher Mach numbers, the sabot described in Ref. 1 was reinforced to ensure that the supports for the model did not fail under the large acceleration loads at launch. This was done by adding drag bars extending from the forward lip of the sabot to the forward model brackets (the latter had previously been merely cantilevered from the side of the sabot) and by providing lateral support to the thrust pad quarters to prevent their spreading apart under the wedge action of "duck's tail" projection at the base of the fuselage. A photograph of the strengthened sabot is shown in Figure 5.

2.2 Model Measurements

In the procedure described in Ref. 4 for measuring model moments of inertia, the product of inertia I_{xz} was found by a series of measurements of the period of the model's oscillation when suspended by a wire from its tail, and swung as a torsion pendulum. For each of the series of measurements, the model was suspended at a slightly different angle to the vertical, and its attitude relative to a plumb line measured by photography while the model was at rest. A considerable improvement to this system in terms of time and accuracy has been made for the Phase 2 models by projecting a shadow of the suspended model onto a circular ground glass screen which can be rotated so that a reticle on the screen is aligned with the fuselage datum from the shadow. The inclination of the model from the vertical can then be read directly from a vernier scale at the edge of the ground glass, see Figure 6.

In addition to the methods described in Ref. 1 for measuring the angles of attack and sideslip from the yaw card cuts, a new device termed the Flight Attitude Shadowgraph was made to interpret the yaw cards from unstable models with attitude angles so large that the required reference points on the cut are poorly defined. A description and photograph of this device are given in Refs. 2 and 13.

3.0 TEST RESULTS

There were originally 12 models in the Phase 2 series, intended to cover the range of Mach numbers from 1.3 to 2.5 as follows:

M = 1.3	M = 2.1
10-13(24ST Alum.)	10-14(75ST Alum.)
10-19(24ST)	10-16(75ST)
	10-21(SPS 245)
M = 1.55	
10-11(24ST Alum.)	**M = 2.5**
	10-15(75ST Alum.)
M = 1.8	10-18(75ST)
	10-22(SPS 245)
10-12(24ST Alum.)	
10-17(24ST)	
10-20(SPS 245 Steel)	

As the models of Phase 1 had all been launched at about Mach 1.6, only one of the second series was tested at this speed, to check the previous results. One steel model was fired at each of the three higher speeds, as it had been found in Phase 1 that a more satisfactory test record for studying the short period longitudinal oscillation could be obtained with the higher density material. It will be noted that for launch speeds above Mach 2, the aluminum models were made of 75ST instead of 24ST to withstand the higher acceleration at launch.

All the models below M = 1.8 were launched successfully and were stable throughout their flight, however the tests showed that 75ST would not stand up to the launch at 2.5, and both models 10-15 and 10-18 struck the edge of the escape hole at the sabot trap. The remaining two of this material, 10-14 and 10-16, were launched successfully at M = 1.9 but were very unstable in flight (see Fig. 8c) such that the data could not be used. Model 10-22 in steel developed a similar instability later in its flight, (see Fig. 8d). Because of the unsuccessful results from the high speed models, three additional aluminum models were prepared, 10-23, -24, and -25. The first two of these were ballasted to obtain good longitudinal results at M = 1.4 and 1.6 while the last was made of 75ST for a launch at M = 2.1 and was fitted with a steel fin in an attempt to avoid the instability of models 10-14 and 10-16. Although the flight was less erratic than for these previous rounds, the same type of instability did appear.

Typical shadowgraphs are shown in Figures 7a, b and c. The plan view of model 10-14 in Figure 7b shows a condition of partial stall over the inboard wing, which resulted from the high angle of attack during the flight. Figure 7a by comparison shows the low turbulence in the wake of an unstalled wing from the flight of 10-19 at low angles of attack. Figure 7c is an interesting side view of model 10-16, showing the boundary layer build-up along the fuselage.

The velocity histories of the successful models are plotted in Ref. 14 and in Figures 8a, b, c and d some of the test records of angles of attack, sideslip and roll are given. Figures 8a and b are for models 10-19 and 10-20 and are typical of the flight records of stable rounds for aluminum and steel models respectively. Figures 8c and d, on the other hand, represent the flight path of models 10-16 and 10-22 which were unstable. Although it is difficult to obtain good accuracy of measurement for attitude angles when the amplitudes are so large, the records show a coupled oscillation in yaw and angle of attack which very quickly becomes divergent reaching angles up to 90^{o}. The analysis of the stable models will be discussed in Section 4.0 and that of the unstable rounds in Section 5.0.

In Appendix A, a brief summary is given of the results of each model, listed in chronological order, and in Table 1 the test data for the successful rounds has been listed. Trajectory data for all rounds is given in Ref. 14.

4.0 ANALYSIS OF STABLE MODELS AND DISCUSSION OF RESULTS

Models 10-11, -12, -13, -17, -19, -20, -21, -23 and -24 were all stable, i.e. their oscillations did not increase substantially in amplitude during the test period, and had little enough cross-coupling between pitch and yaw that the methods of analysis of Refs. 1 and 2 could be used. As the methods are described fully in these references, no further description will be given here.

The results of the lateral analysis are plotted in Figure 9a and b as graphs of the derivatives C_{n_β}, C_{l_β}, C_{n_p} and C_{l_p} vs. Mach number. The longitudinal analysis included calculations of derivatives C_{M_α}, and $(C_{M_{\dot{\alpha}}} + C_{M_q})$, and the total drag coefficient C_D. These are plotted vs. Mach number in Figures 10 and 11.

For C_{n_β} and C_{l_β} it will be noted that there is fairly good agreement with the results of NACA wind tunnel tests, and with Avro's 1/8th scale free flight tests. Although a more recent Avro report (Ref. 8) was available, the earlier data of Refs. 5 and 6 were plotted here as they show the results of the two test methods separately rather than combining them into a single curve.

For C_{n_p} there is a large disagreement with the results of the free flight tests as reported in Ref. 8, although the latter are at variance with the positive values given earlier in Ref. 6 (see Fig. 11b of Ref. 1). Values of C_{l_p} show little scatter, and fall very close to an early Avro estimate, but are below the free flight values of Ref. 8 and the NAE wind tunnel result of Ref. 7. The latter result was obtained using Mr. Orlik-Rückemann's technique of free oscillation with feedback excitation as described in Ref. 9 with a model prepared by CARDE identical to the aeroballistic models. It is hoped that by a continuation of the NAE tests, values of C_{n_p} can be obtained for comparison with the CARDE results.

Values of C_{M_α} as shown in Figure 10 are somewhat lower than those from either the free flight models or the wind tunnel tests but they do exhibit the same trend with Mach number. Although few of the records of angle of attack were suitable for a measurement of damping, the values of $(C_{M_{\dot\alpha}} + C_{M_q})$ so obtained are seen to lie in general between the free flight curve and the earlier estimate of Ref. 10. The CARDE results have been reduced to a centre of gravity position of 27% mean aerodynamic chord with the aid of cross plots of $(C_{M_{\dot\alpha}} + C_{M_q})$ vs. center of gravity position from Ref. 10.

Total drag coefficient C_D is plotted in Figure 11, using the decelerations measured from the velocity records given in Ref. 14. No attempt has been made to break this drag down into component types of drag; however, to give a comparison with the drag information in Ref. 11 based on NACA wind tunnel and free flight tests, two curves have been drawn on Figure 11 showing the sum of profile, induced and elevator drag obtained from Ref. 11 for the cases of mean angles of attack of 2° and 3° and an elevator deflection angle of 7 degrees. This represents a typical range of angles for the CARDE models and it will be noted that the CARDE values in general fall between these two lines, showing a good agreement in drag with the Avro result.

5.0 ANALYSIS OF UNSTABLE MODELS AND DISCUSSION OF RESULTS

Models 10-14, -16, -22 and -25 all exhibited instability of the type shown in Figures 8c and d. As this violent type of motion occurred at Mach numbers as low as 1.92, which is well within the speed range of the full-scale aircraft, Avro Aircraft Ltd. were advised of the test results, and through the co-operation of Mr. S.F. Kwiatkowski, they undertook an analysis program to find the cause of the instability. Only the essentials of this study will be given here, as a complete description could form the subject of a separate report.

Avro were provided with an aluminum fin and rudder which they subjected to load-deflection tests to determine the aeroelastic effects which could be expected during the aeroballistic range flights. At a station position 80% span from the root, the measured influence coefficients were:

$$\frac{\theta}{P} = 6.72 \times 10^{-3} \text{ rad/lb. for bending loads,}$$

$$\frac{\theta}{T} = 13.57 \times 10^{-3} \text{ rad/in.lb. for torque loads.}$$

From these values, it was estimated that aeroelastic effects would cause a 10% reduction in C_{n_β} and C_{y_β}.

Using the inertia and geometry characteristics and range atmosphere data for model 10-16, a complete set of rigid aerodynamic derivatives were estimated for the full seven degree of freedom equations as listed in Appendix B (for notation see Ref. 12). The IBM 704 digital computer

was then programmed to calculate angles of attack, sideslip and roll using these equations. The resulting plots are given in Figures 12, 13 and 14 labelled as the first estimate, together with the actual test points from model 10-16. It will be noted that for the first estimate, using rigid derivatives, neither α nor β reaches excessive values.

For the second estimate shown in Figures 12 to 14, the values of C_{y_β} and C_{n_β} reduced by 10% were used, with all other derivatives the same as for the first estimate. This time the calculated α and β histories follow the test points more closely, with the angle of attack diverging within 0.02 seconds.

The third estimate plotted represents an additional 20% decrease of C_{n_β} and C_{y_β}, with the other derivatives still remaining at their rigid values. In the case of α and β, the calculated values diverge more widely than the test points, while a somewhat closer agreement to the roll angle ϕ is obtained.

The results of the Avro study thus indicate that the instability experienced by the high speed models is caused by the aeroelastic effects on the tail fin. Based on this investigation, all the remaining high speed models were modified by replacing the aluminum fins with steel ones which would have greater stiffness. Despite this, both the steel model 10-22, launched at Mach 2.5, and the modified aluminum model 10-25 at Mach 2.1 again developed very large attitude angles during their flight, indicating that some aeroelastic effect is still present with a steel fin. It would appear therefore that with thin winged models of this type, further attention should be paid to the aeroelastic problems which can arise at high launch speeds.

Having thus obtained a reasonable agreement with the CARDE test results using the aeroelastic influence coefficients measured from the model fin, Avro calculated by a similar procedure the behaviour of the full-scale aircraft using full scale values for the aeroelastic constants, and found that there was no likelihood of such violent motions occurring within their flight envelope.

6.0 CONCLUSIONS

The second and final phase of tests on 1/120th scale aeroballistic models of the CF-105 has been completed with the launching of 15 models at speeds from Mach 1.38 to 2.5. These models were made of aluminum or steel using a pantograph milling machine (Die Sinker) from new masters representing the latest Mk II configuration of the CF-105. Improved methods of checking wing profiles and fuselage sections were adopted for the Phase 2 tests. Whereas the purpose of the first phase of these tests, as reported in Ref. 1, was to develop procedures for manufacture, testing and analysis of the models, Phase 2 was intended to obtain useful aerodynamic information about the aircraft over a range of speeds extending to beyond that of any of the previous test methods for the aircraft. This study suggests that the range technique might

be extended to provide a means of investigating the possibility of instability due to aeroelastic distortion as a basic part of the test program of very high speed aircraft.

Although the difficult problem of successfully launching models of this type, having very little base area, at high speed has been overcome through the use of high strength steels, all of the models tested at speeds above Mach 2 failed to produce specific values of stability derivatives because of a form of instability resulting in very large amplitude oscillations in pitch and sideslip. To investigate this phenomenon, an analysis program was carried out by Avro Aircraft which consisted essentially of calculating flight histories on the IBM 704 computer by substituting estimated derivative values into the full seven degree of freedom equations of motion. It was found that histories of pitch, yaw and roll quite similar to the test results could be obtained by using values of C_{n_β} and C_{y_β} reduced by about 10% from the estimates for a rigid aircraft. It was determined experimentally that such a reduction would result from aeroelastic effects on the model fin and rudder. Calculations showed however that such violent manoeuvres were unlikely to occur with the full scale aircraft.

At speeds below Mach 2.0, all the models were launched successfully and were stable throughout their flight. Values of lateral and longitudinal stability derivatives obtained from these tests were generally in good agreement with the results of large scale free-flight model tests and high speed wind-tunnel tests. The total drag coefficients calculated from the measured model retardations agreed very well with current Avro values for the same speed, elevator deflection and mean angle of attack.

ACKNOWLEDGEMENTS

The authors wish to acknowledge the co-operation and assistance given to this program by Mr. K. Orlik-Rückemann and his staff at the High Speed Aeronautical Laboratory of the National Aeronautical Establishment, and Mr. S.F. Kwiatkowski, Head of the Stability and Control Section of Avro Aircraft Limited.

REFERENCES

1. H.R. Warren — Aeroballistics Range Tests of the CF-105 Phase 1 - Rounds 1 to 10 CARDE TM AB-43, March 1958

2. H.R. Warren — Aeroballistics Range Measurements of the Performance and Stability of Supersonic Aircraft CARDE TM AB-32, June 1958

3. L.J. Crowe, Avro Aircraft Ltd. — CF-105 Aircraft Geometry Report AVRO P/GEOM/32

4. H.R. Warren — Measurement of Model Aeroplane Moments and Products of Inertia CARDE TM AB-31, September 1957

5. Avro Aircraft Ltd. — CF-105 Rigid Lateral Derivatives from Wind Tunnel Tests. M = 0.5 to M = 2.0 AVRO P/Aero Data/81, March 1956

6. Avro Aircraft Ltd. — Free Flight Model Derivatives Converted to CF-105 Configuration AVRO P/FFM/56, July 1957

7. Unpublished NAE Wind Tunnel tests of the CF-105 Aircraft

8. Avro Aircraft Ltd. — CF-105 Elastic Lateral Derivatives from Wind Tunnel and Free Flight Model Tests AVRO P/Aero Data/97, July 1957

9. K. Orlik-Rückemann — Methods of Measurement of Aircraft Dynamic Stability Derivatives NAE Quarterly Bulletin Report No. NAE 1957(4), December 1957

10. Avro Aircraft Ltd. — CF-105 Rigid Longitudinal Derivatives from Wind Tunnel Tests to Mach 2.0 and Theory AVRO P/Aero Data/84, November 1956

11. Avro Aircraft Ltd. — CF-105 Rigid Longitudinal Derivatives AVRO P/Aero Data/98, September 1957

12. Avro Aircraft Ltd. — Digital Computation of Response Predictions in 7 Degrees of Freedom AVRO 71/Stab/37, June 1958

13. F.B. Snelgrove — Flight Attitude Shadowgraph CARDE TL 1199/59, May 1959

14. B. Cheers — Data Report on CF-105 Aeroballistics Range Models. Phase 2 - Models 10-11 to 10-25 CARDE TL to be published later

APPENDIX A

SUMMARY OF TEST DATA

In this Appendix, a brief summary is first given of the results of each model, listed in chronological order, and then, in Table I, the model geometry and inertia characteristics and the range atmosphere data are listed for the successful rounds.

Model 10-11. Tested February 7, 1958, at M = 1.64 this model was to provide a check on the models launched at about this speed in Phase 1. The previous results were confirmed, all derivative values coming close to those of Phase 1.

Model 10-12. Tested February 19, 1958, at M = 1.81, this model showed typical Dutch roll coupling of yaw and roll with no sign of the instability which occurred at only slightly higher speed with models 10-14 and -16.

Model 10-13. Tested February 19, 1958, at M = 1.38, this model again showed similar flight behaviour to that of the models of Phase 1.

On the basis of these three tests, it was decided to proceed with a high speed test at Mach 2.5.

Model 10-15. Tested April 23, 1958, at M = 2.5, this model was made of 75ST aluminum rather than the 24ST of the previous models to increase its resistance to the higher acceleration loads of high speed launch. The model did not launch satisfactorily, however, and struck the edge of the escape hole at the sabot trap.

Model 10-16. Tested May 16, 1958, at M = 1.94, this model also was made of 75ST aluminum. The launch was successful, and the model entered the range at the usual small pitch and yaw angles but quickly attained a high roll rate of approximately 18°/ft. followed by a rapid divergence in the amplitudes of the pitch and yaw angles, reaching values of 90° (see Figures 7c and 8c).

Model 10-14. Tested July 4, 1958, at M = 1.92, was made of 75ST but differed from 10-16 in that Hevimet high density ballast material was used to alter the inclination of the principal longitudinal axis of inertia. It was thought at that time that the erratic behaviour of 10-16 could have been caused by an inertia cross-coupling effect. The ballast, distributed as shown in Figure 6, reduced the product of inertia I_{xz} to 0, but despite this, the same type of instability developed. Unfortunately the large block of Hevimet located beneath the fin and rudder separated from the fuselage at Station 133, so that results beyond that point have no significance. The record shows however that the roll rate prior to this point was almost the same as for 10-16 and the divergence in pitch and yaw had commenced.

Model 10-20. Tested August 29, 1958, at M = 1.7, this model was made of high strength SPS 245 steel (yield point 108,000 psi) as a means of increasing the wavelength of oscillations and thereby obtaining more points per cycle. As a result of Avro's suggestion that fin aeroelastic effects were to blame for the unstable flights of 10-16 and 10-14, the aluminum fin planned for this model was replaced by a steel one. As shown in Figure 10b, a very useful record was obtained, particularly of the angle of attack.

Model 10-21. Tested September 12, 1958, at M = 1.97, again made of steel throughout, this model flew the entire length of the range with no sign of the instability which occurred with 10-16, although the speed was somewhat higher. This seemed to confirm the explanation of fin flexibility.

Model 10-17. Tested November 25, 1958, at M = 1.68, this model was made of 25ST aluminum. It flew with very little oscillation in pitch, and a very clearly defined Dutch roll oscillation in yaw and roll with approximately zero damping.

Model 10-19. Tested November 25, 1958, at M = 1.50, the model was made of 24ST aluminum and as shown in Figures 7a and 8a, a stable flight resulted, with useful records of pitch, roll and yaw. It might be noted that for records such as this one, the measurements of frequency, damping, phase and amplitude for the roll angle ϕ are not taken from the record shown, but from a plot made of the difference between the measured value of ϕ and the calculated value of a straight line mean value such as the one shown dotted. In this way, full advantage can be taken of the accuracy with which the roll angle is measured.

Model 10-22. Tested November 26, 1958, at M = 2.5, this model was made of SPS245 steel throughout and was the first model to be successfully launched at this speed. The resulting record, (see Figure 8d) shows some very interesting features. After the model had passed station 180, a divergent type of oscillation occurred similar to that of 10-14 and 10-16. Prior to this point, however, there were several oscillations in pitch and yaw of fairly small amplitude which did not diverge. One curious point about these oscillations is that their wavelength is much less than that of 10-20 (Figure 8b) which was also made of steel, the wavelengths of β being about 34% of the previous value and α about 56% of the value for 10-20. The roll record shows a similar characteristic to that of 10-16, with a gradual build up in rate, but practically no trace of an oscillation. This round would be a good subject for further study since the aeroelastic effects should have been minimized with an all steel model and yet the same type of instability developed as for the aluminum models 10-14 and 10-16.

Model 10-18. Tested February 11, 1959, at M = 2.3, this model was made of 75ST aluminum but was ballasted to reduce the product of inertia, and fitted with a steel fin to reduce aeroelastic effects. Unfortunately there was a disturbance at launch, apparently similar to that of model 10-15, which caused the model to strike the edge of the escape hole at the sabot trap.

Model 10-25. Tested February 11, 1959, at M = 2.1, this model was made of 75ST and, like 10-18, was ballasted and fitted with a fin made of SPS245 steel. The launch was successful but the model developed the same type of instability as 10-14 and 10-16.

Model 10-23. Tested March 19, 1959, at M = 1.49, the model was made of 75ST and ballasted to reduce the product of inertia. The flight was successful and good longitudinal and lateral results were obtained.

Model 10-24. Tested March 19, 1959, at M = 1.71, this model was made like 10-23 and also gave good lateral and longitudinal results.

APPENDIX A

TABLE I

MODEL GEOMETRY AND RANGE ATMOSPHERE DATA

MODEL NO.			10-11	10-12	10-13	10-14	10-16	10-17	10-19	10-20	10-21	10-23	10-24
Wing Area	S	sq. in.	12.24	12.22	12.34	12.52	12.25	12.29	12.45	12.52	12.48	12.42	12.47
Wing Span	b	in.	5.000	5.002	5.006	5.000	5.000	5.000	5.000	5.001	5.000	5.001	4.998
Length of Mean Aerodynamic Chord	$\bar{c}$	in.	3.030	3.009	3.027	3.067	3.022	3.018	3.062	3.070	3.062	3.025	3.016
CG Position	$\%\bar{c}$		14.2	15.4	14.8	21.4	15.7	15.8	16.7	18.9	18.2	13.9	14.1
Elevator Deflection		deg.	7	8.3	5	7	7	8.3	5	8.3	7	5	5
Model Material			24ST ALUM.	24ST ALUM.	24ST ALUM.	75ST ALUM.	75ST ALUM.	24ST ALUM.	24ST ALUM.	SPS245 STEEL	SPS245 STEEL	75ST ALUM.	75ST ALUM.
Ballast Material			NIL	NIL	NIL	HEVIMET	NIL	NIL	NIL	NIL	NIL	HEVIMET	HEVIMET
Weight		lb.	0.286	0.280	0.274	.348	.289	.281	.281	.789	.745	0.293	0.292
I_x		$lb.in.^2$	0.0908	0.0839	0.0754	0.0991	0.0922	0.0917	0.0914	0.2833	0.2355	0.09640	0.09758
I_y		$lb.in.^2$	0.804	0.801	0.785	1.325	0.813	0.795	0.742	2.128	2.004	0.823	0.833
I_z		$lb.in.^2$	0.870	0.844	0.834	1.314	0.878	0.853	0.835	2.352	2.202	0.872	0.837
I_{xz}		$lb.in.^2$	0.0227	0.01970	0.0364	0	0.01590	0.01590	0.01725	0.04315	0.04207	0.00964	0.0104
Date of Test			7.2.58	19.2.58	19.2.58	4.7.58	16.5.58	25.11.58	25.11.58	29.8.58	12.9.58	19.3.59	19.3.59
Range Temperature		^oF	20	18	18	68	54	28	32	72	55	26	28
Range Speed of Sound		ft/sec.	1074	1072	1072	1126	1111	1083	1088	1132	1114	1080	1083
Range Pressure		in.Hg.	29.02	28.79	28.79	29.37	29.36	29.78	29.80	29.26	29.40	29.19	29.20
Range Density		slugs/cu.ft.	.00250	.00249	.00249	.00230	.00236	.00251	.00250	.00226	.00235	.00248	.00247
Mach No. at Entry to Range			1.64	1.81	1.38	1.92	1.94	1.68	1.50	1.7	1.97	1.49	1.71

APPENDIX B

EQUATIONS USED IN AVRO ANALYSIS

A description of the analysis carried out by Avro Aircraft Ltd. on the unstable round 10-16 was given in section 5.0.

A list is given here of the equations of motion which were programmed for the IBM 704 computer for this analysis. The notation is given in Ref. 12.

$$\dot{V} = \sec\alpha \cdot V\left\{\frac{X}{V_m}\sec\beta - g\cdot\frac{\sin\theta\cdot\sec\beta}{V} + \tan\beta\cdot\cos\alpha\cdot\dot{\beta}\right.$$

$$\left. + \sin\alpha\cdot\dot{\alpha} + r\cdot\tan\beta - q\sin\alpha\right\}$$

$$\dot{\alpha} = \sec\alpha\left\{\frac{Z\cdot\sec\beta}{V_m} - \frac{\dot{V}}{V}\sin\alpha + \sin\alpha\cdot\tan\beta\cdot\dot{\beta}\right.$$

$$\left. + q\cdot\cos\alpha - p\cdot\tan\beta + g\frac{\cos\theta\cdot\cos\phi\cdot\sec\beta}{V}\right\}$$

$$\dot{q} = \frac{M}{I_y} - p\cdot r\cdot\left[\frac{I_x - I_z}{I_y}\right] - (p^2 - r^2)\frac{I_{xz}}{I_y}$$

$$\dot{\beta} = \frac{Y\cdot\sec\beta}{V_m} - \frac{\dot{V}}{V}\tan\beta + p\sin\alpha - r\cdot\cos\alpha + \frac{g\cdot\sin\phi\cos\theta\sec\beta}{V}$$

$$\dot{p} = \frac{L}{I_x} - q\cdot r\,\frac{(I_z - I_y)}{I_x} + (\dot{r} + q\cdot p)\frac{I_{xz}}{I_x}$$

$$\dot{r} = \frac{N}{I_z} - p\cdot q\,\frac{(I_y - I_x)}{I_z} - (q\cdot r - \dot{p})\,\frac{I_{xz}}{I_z}$$

$$\dot{h} = V(\cos\alpha\cdot\cos\beta\cdot\sin\theta - \cos\beta\cdot\sin\alpha\cdot\cos\theta\cdot\cos\phi - \sin\beta\cdot\cos\theta\cdot\sin\phi)$$

$$a = a_1 + \frac{\partial a}{\partial h}\cdot h \geqslant a_s = \text{Speed of sound in the stratosphere}$$

$$\rho = \rho_1 + \frac{\partial\rho}{\partial h}\cdot h$$

$$H = H_1 + h \qquad \text{Note } h_1 = 0$$

$$\dot{\phi} = p + \tan\theta \left(q \cdot \sin\phi + r \cdot \cos\phi \right)$$

$$\dot{\theta} = q \cos\phi - r \cdot \sin\phi$$

$$\dot{V}_1' = \sec\alpha \cdot V \left\{ \frac{X}{V_m} \cdot \sec\beta - g \frac{\sin\theta \cdot \sec\beta}{V} + r \tan\beta - q \sin\alpha \right\}$$

$$\dot{p}_1' = \left\{ \frac{L}{I_x} - q \cdot r \cdot \frac{(I_z - I_y)}{I_x} + q \cdot p \cdot \frac{I_{xz}}{I_x} \right\}$$

$$\dot{\psi} = q \cdot \sin\phi \cdot \sec\theta + r \cdot \sec\theta \cdot \cos\phi$$

$$n = \frac{-Z}{mg}$$

$$n_y = \frac{+Y}{mg}$$

$$\delta_a = 1/2 \left[\delta_{a_s} - \delta_{a_p} \right]$$

$$\delta_{a_e} = 1/2 \left[\delta_{a_s} + \delta_{a_p} \right]$$

$$X = 1/2 \rho V^2 S \left\{ Cx_1 + (\alpha - \alpha_1) Cx_\alpha + (\alpha - \alpha_1)^2 \frac{Cx}{2}\alpha_\alpha + \alpha Cx_{\alpha_m}, (M' - M_1') \right.$$

$$+ \dot{\alpha} Cx_{\dot{\alpha}} \frac{\bar{c}}{2V} + qCxq \frac{\bar{c}}{2V} + C_{x_{oM'}} (M' - M_1') + C_{x\delta_{a_e}} \cdot \delta_{a_e}$$

$$+ (\delta_a - \delta_{a_1}) Cx\delta_a + (\delta_e - \delta_{e_1}) Cx\delta_e + (\delta_r - \delta_{r_1}) Cx\delta_r$$

$$\left. + \delta_e \cdot C_{x\delta_{eM'}} (M' - M_1') \right\} + \cos i \left\{ (2T - T_1) + (\alpha - \alpha_1) \frac{\partial T}{\partial \alpha} + (V - V_1) \frac{\partial T}{\partial V} + \frac{\partial T}{\partial h} \cdot h \right\}$$

$$Z = 1/2 \rho V^2 S \left\{ Cz_1 + (\alpha - \alpha_1) Cz_\alpha + (\alpha - \alpha_1)^2 \frac{Cz}{2}\alpha_\alpha + \alpha Cz_{\alpha_m}, (M' - M_1') \right.$$

$$\left. + \dot{\alpha} Cz_{\dot{\alpha}} \frac{\bar{c}}{2V} + qCz_q \frac{\bar{c}}{2V} + Cz_{\delta_{a_e}} \cdot \delta a_e + \delta_e Cz_{\delta_{e_{M'}}} (M' - M_1') + \right.$$

$$+ (\delta_a - \delta_{a_1})Cz\delta_a + (\delta_e - \delta_{e_1})Cz\delta_e + (\delta_r - \delta_{r_1})Cz\delta_r \Big\}$$

$$+ \sin i \left\{ (2T-T_1) + (\alpha-\alpha_1)\frac{\partial T}{\partial \alpha} + (V-V_1)\frac{\partial T}{\partial V} + \frac{\partial T}{\partial h} \cdot h \right\}$$

$$M = 1/2\,\rho V^2 S\bar{c} \Big\{ Cm_1 + (\alpha-\alpha_1)Cm_\alpha + (\alpha-\alpha_1)^2 \frac{Cm_\alpha}{2} + Cm_{\delta_{ae}} \cdot \delta a_e$$

$$+ \alpha Cm_{\alpha_{M'}}(M' - M_1') + \dot{\alpha} Cm_{\dot{\alpha}} \frac{\bar{c}}{2V} + qCm_q \frac{\bar{c}}{2V} + \delta_e\, Cm_{\delta_{eM'}}(M' - M_1')$$

$$+ (\delta_a - \delta_{a_1})\, Cm\delta_a + (\delta_e - \delta_{e_1})\, Cm\delta_e + (\delta_r - \delta_{r_1})\, Cm\delta_r \Big\}$$

$$+ e \left\{ (2T-T_1) + (\alpha-\alpha_1)\frac{\partial T}{\partial \alpha} + (V-V_1)\frac{\partial T}{\partial V} + \frac{\partial T}{\partial h} \cdot h \right\}$$

$$Y = 1/2\,\rho V^2 S \Big\{ C_Y + (\beta-\beta_1)C_{Y_\beta} + (\beta-\beta_1)^2 \frac{C_{Y_\beta}}{2} + \beta C_{Y_{\beta_\alpha}}(\alpha-\alpha_1)$$

$$+ \beta\, C_{Y_{\beta_{M'}}}(M' - M_1') + \dot{\beta} \cdot C_{Y_{\dot{\beta}}} \frac{b}{2V} + pC_{Y_p} \frac{b}{2V} + r\, C_{Y_r} \frac{b}{2V}$$

$$+ (\delta_a - \delta_{a_1})\, C_{Y\delta_a} + (\delta_e - \delta_{e_1})\, C_{Y\delta_e} + (\delta_r - \delta_{r_1})C_{Y\delta_r}$$

$$+ \delta_a\, C_{Y\delta_{a_\alpha}}(\alpha-\alpha_1) + \delta_r\, C_{Y\delta_{r_\alpha}}(\alpha-\alpha_1) + \delta_r\, C_{Y\delta_{r_{M'}}}(M' - M_1') \Big\}$$

$$L = 1/2\,\rho V^2 Sb \Big\{ C_{\ell_1} + (\beta-\beta_1)C_{\ell_\beta} + (\beta-\beta_1)^2 \frac{C_{\ell_\beta}}{2} + \beta C_{\ell_{\beta_\alpha}}(\alpha-\alpha_1)$$

$$+ \beta\, C_{\ell_{\beta_{M'}}}(M' - M_1') + \dot{\beta} C_{\ell_{\dot{\beta}}} \frac{b}{2V} + pC_{\ell_p} \frac{b}{2V} + rC_{\ell_r} \frac{b}{2V}$$

$$+ (\delta_a - \delta_{a_1})\, C_{\ell\delta_a} + (\delta_e - \delta_{e_1})\, C_{\ell\delta_e} + (\delta_r - \delta_{r_1})\, C_{\ell\delta_r}$$

$$+ \delta_a\, C_{\ell\delta_{a_{M'}}}(M' - M_1') + \delta_a\, C_{\ell\delta_{a_\alpha}}(\alpha-\alpha_1) \Big\}$$

$$N = 1/2\,\rho V^2 Sb \Big\{ C_{n_1} + (\beta-\beta_1)\, C_{n_\beta} + (\beta-\beta_1)^2 \frac{C_{n_\beta}}{2} + \beta C_{n_{\beta_\alpha}}(\alpha-\alpha_1)$$

$$+ \beta\, C_{n_{\beta_{M'}}}(M' - M_1') + \dot{\beta}\, C_{n_{\dot{\beta}}} \frac{b}{2V} + pC_{n_p} \frac{b}{2V} + r\, C_{n_r} \frac{b}{2V}$$

$$+ (\delta_a - \delta_{a_1})\, C_{n\delta_a} + (\delta_e - \delta_{e_1})\, C_{n\delta_e} + (\delta_r - \delta_{r_1})\, C_{n\delta_r}$$

$$+ \delta_r\, C_{n\delta_{r_M}}(M' - M_1') + \delta_a\, C_{n\delta_{a_\alpha}}(\alpha-\alpha_1) + \delta_r\, C_{n\delta_{r_\alpha}}(\alpha-\alpha_1) \Big\}$$

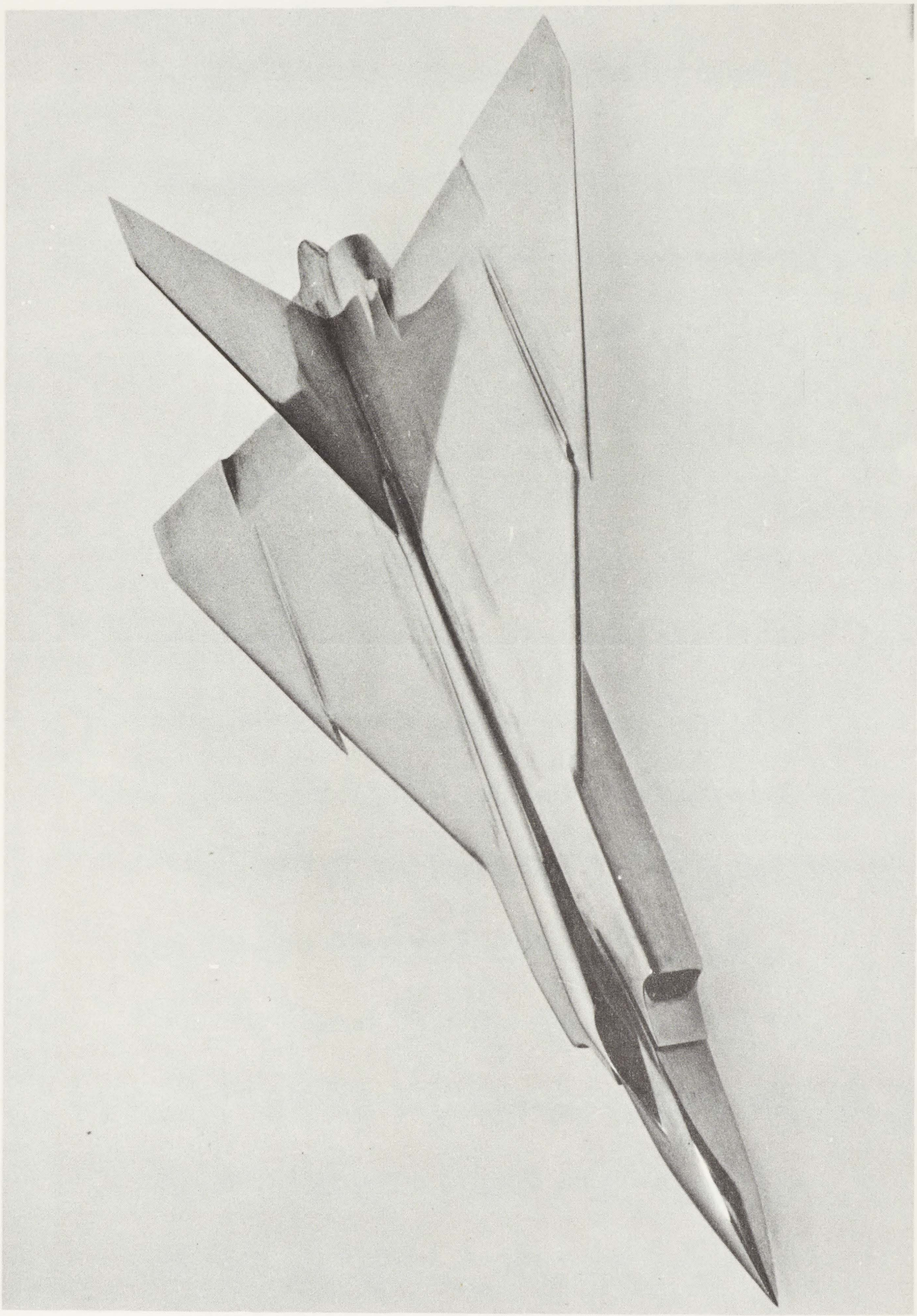

FRONT VIEW OF CF-105 MODEL

FIGURE 1

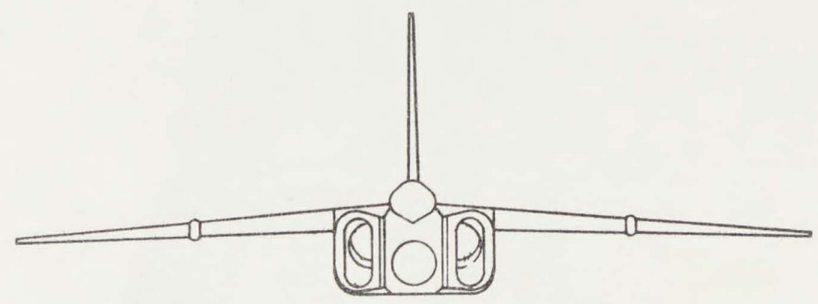

FRONT VIEW

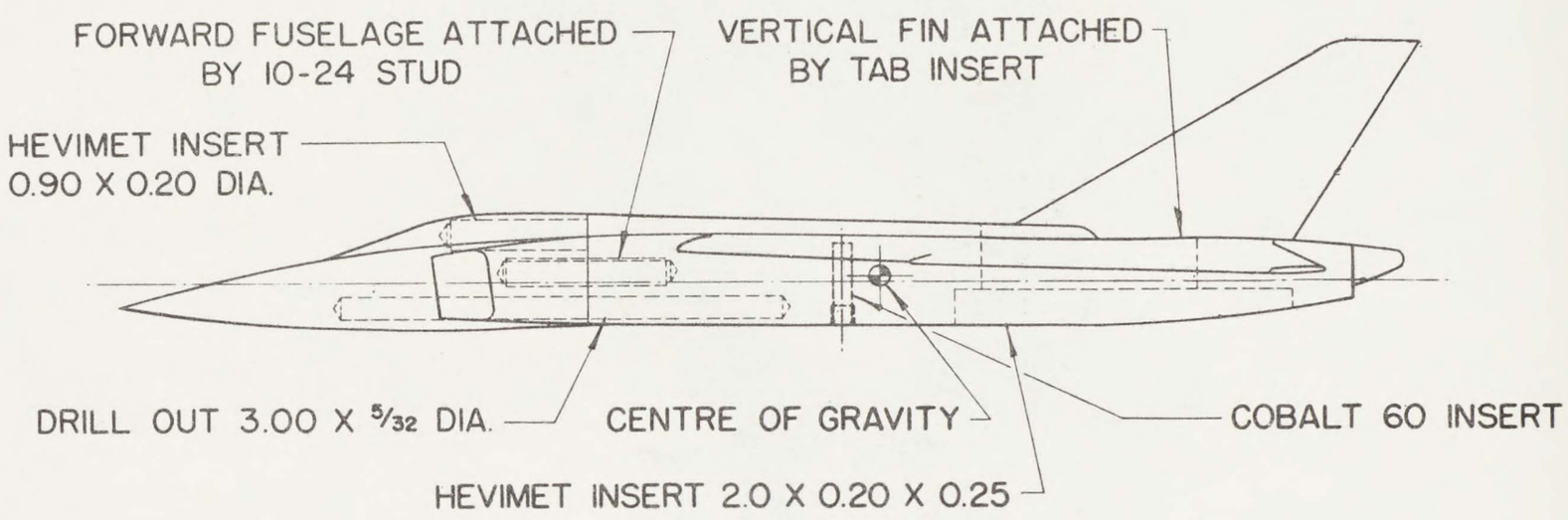

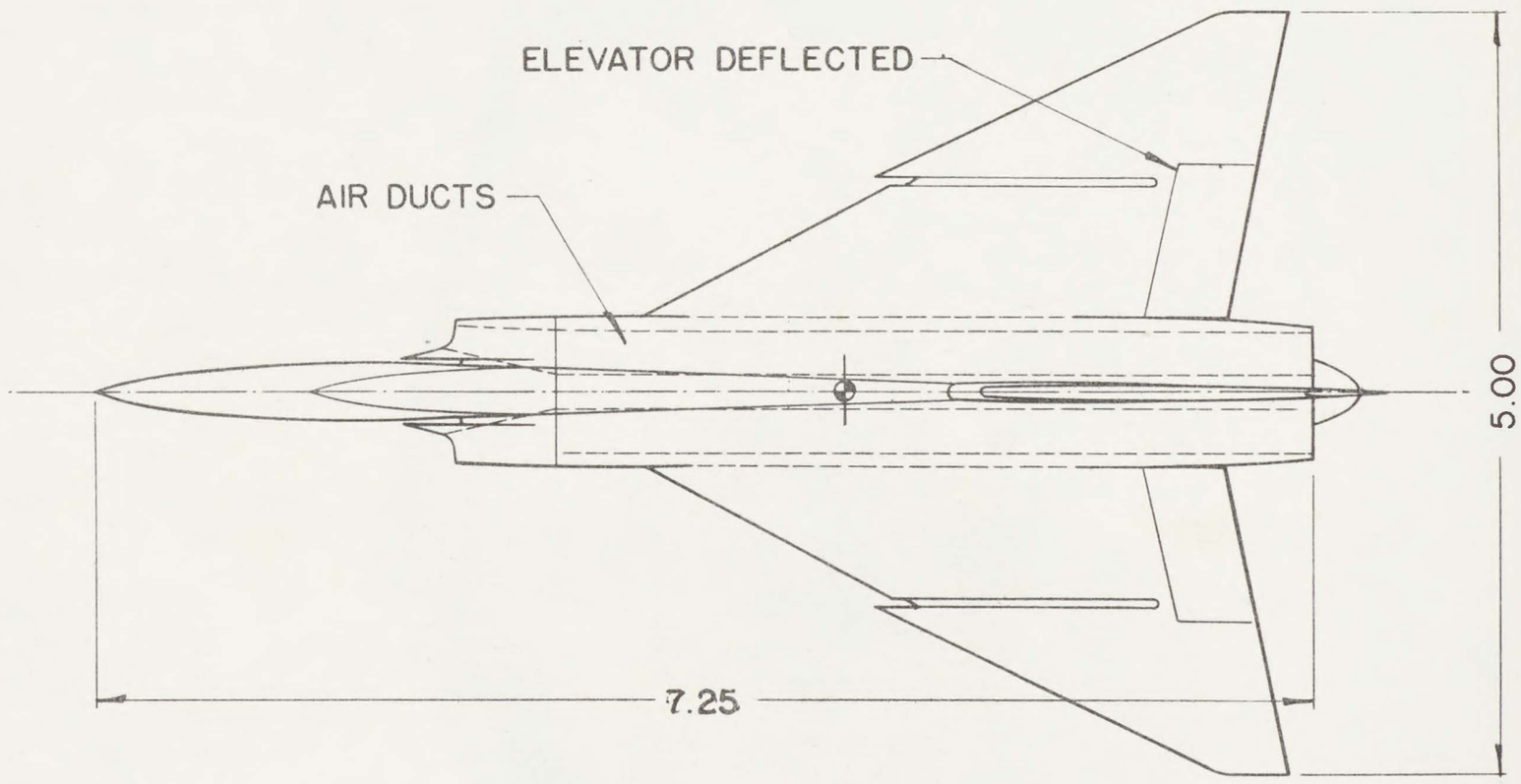

DETAILS OF CONSTRUCTION OF CF-105 MODEL

FIGURE 3

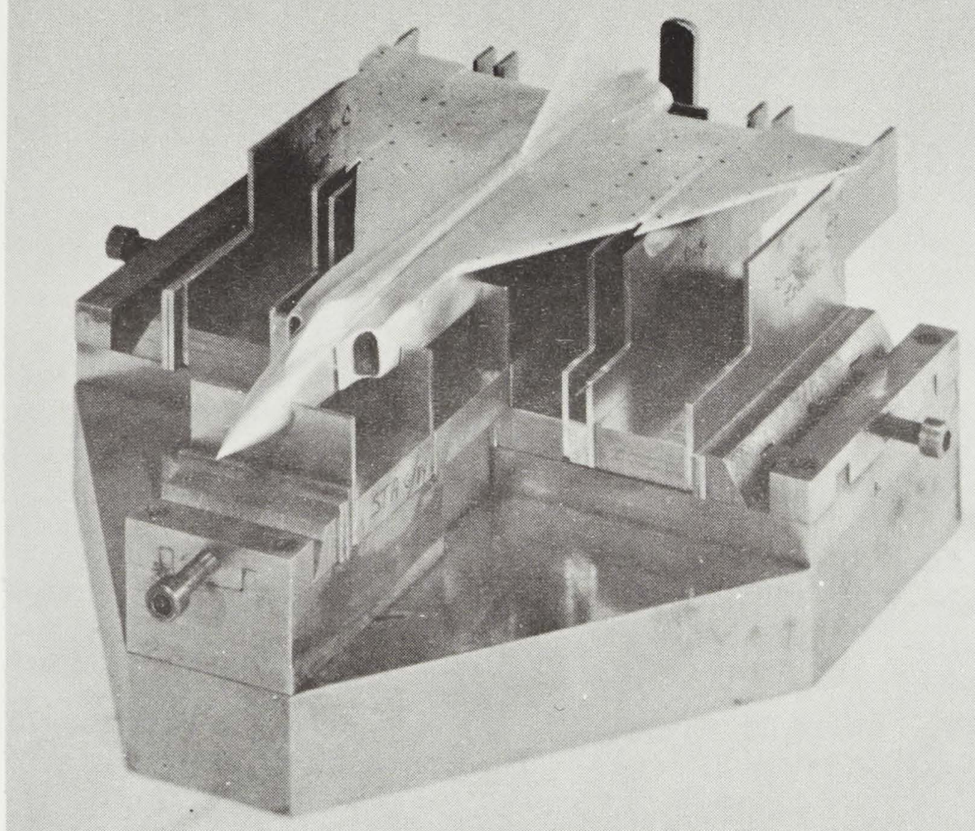

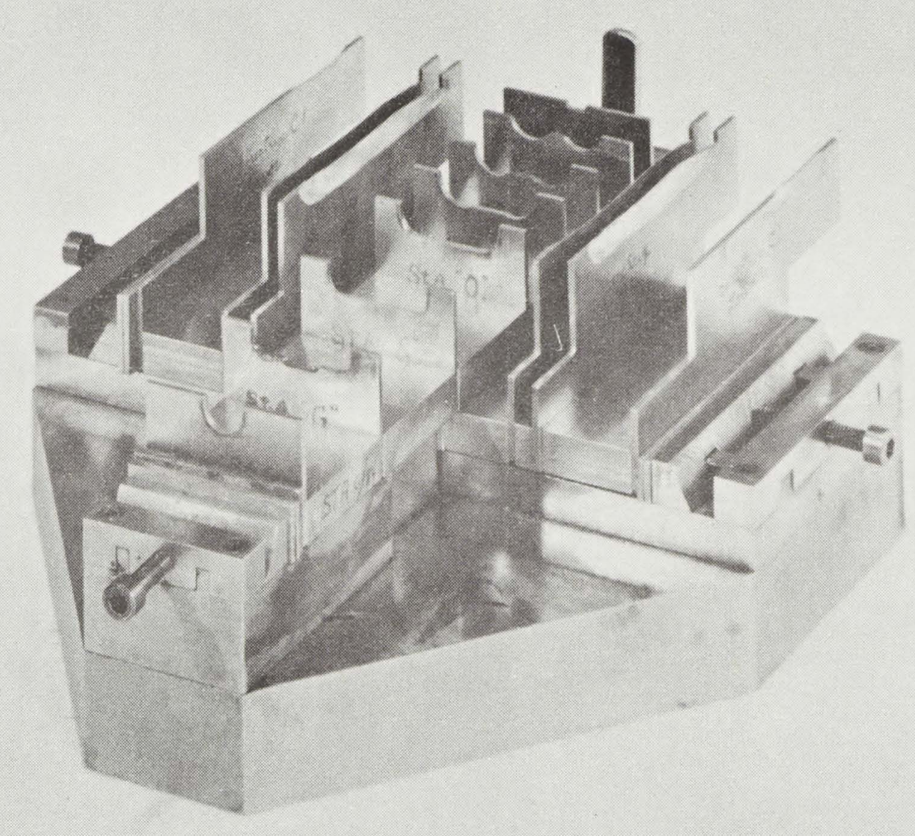

UNCLASSIFIED
CARDE
PHOTO GROUP
NEG NO 13566, 13568

TEMPLATE JIG

FIGURE 4

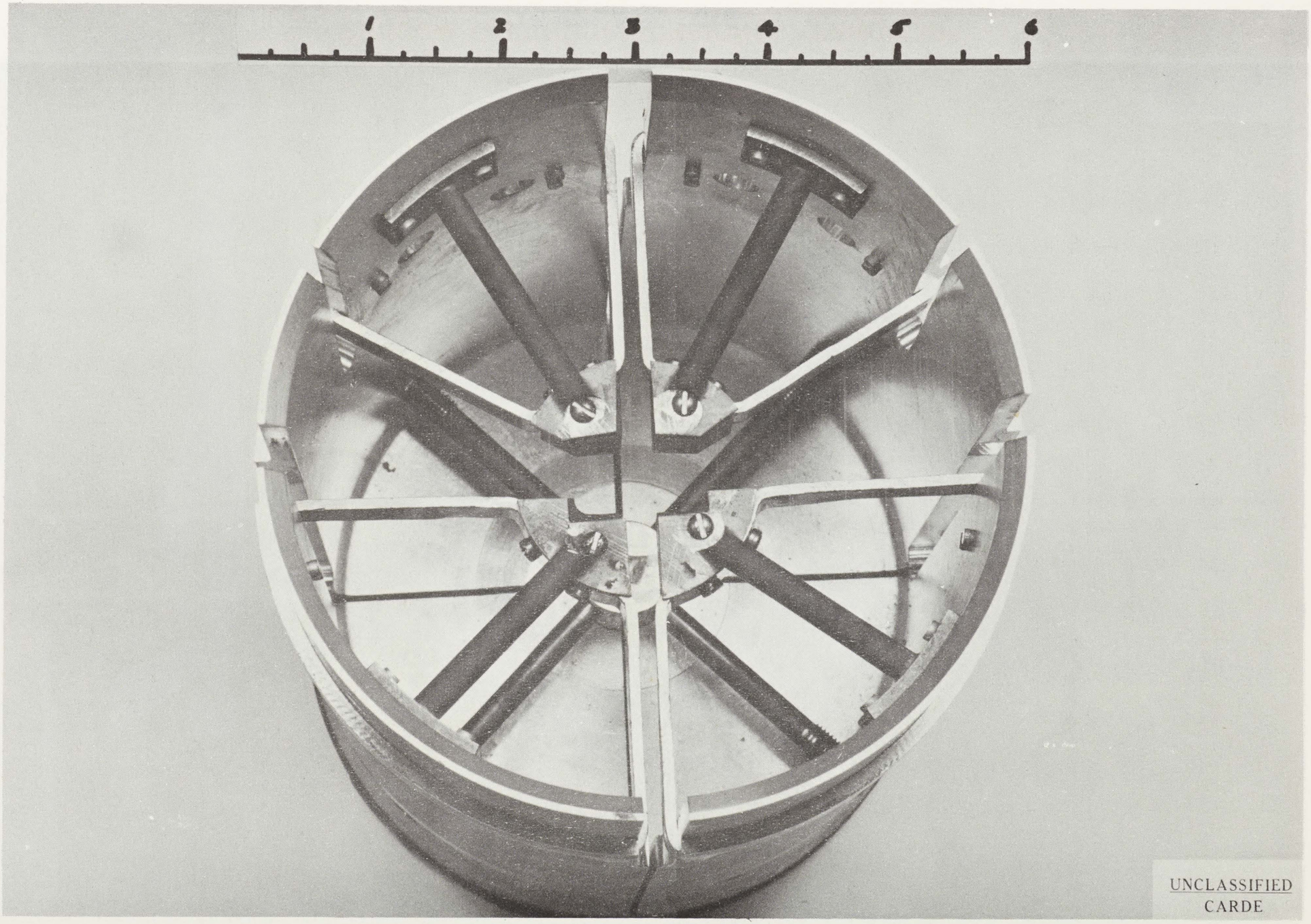

UNCLASSIFIED
CARDE

STRENGTHENED SABOT

FIGURE 5

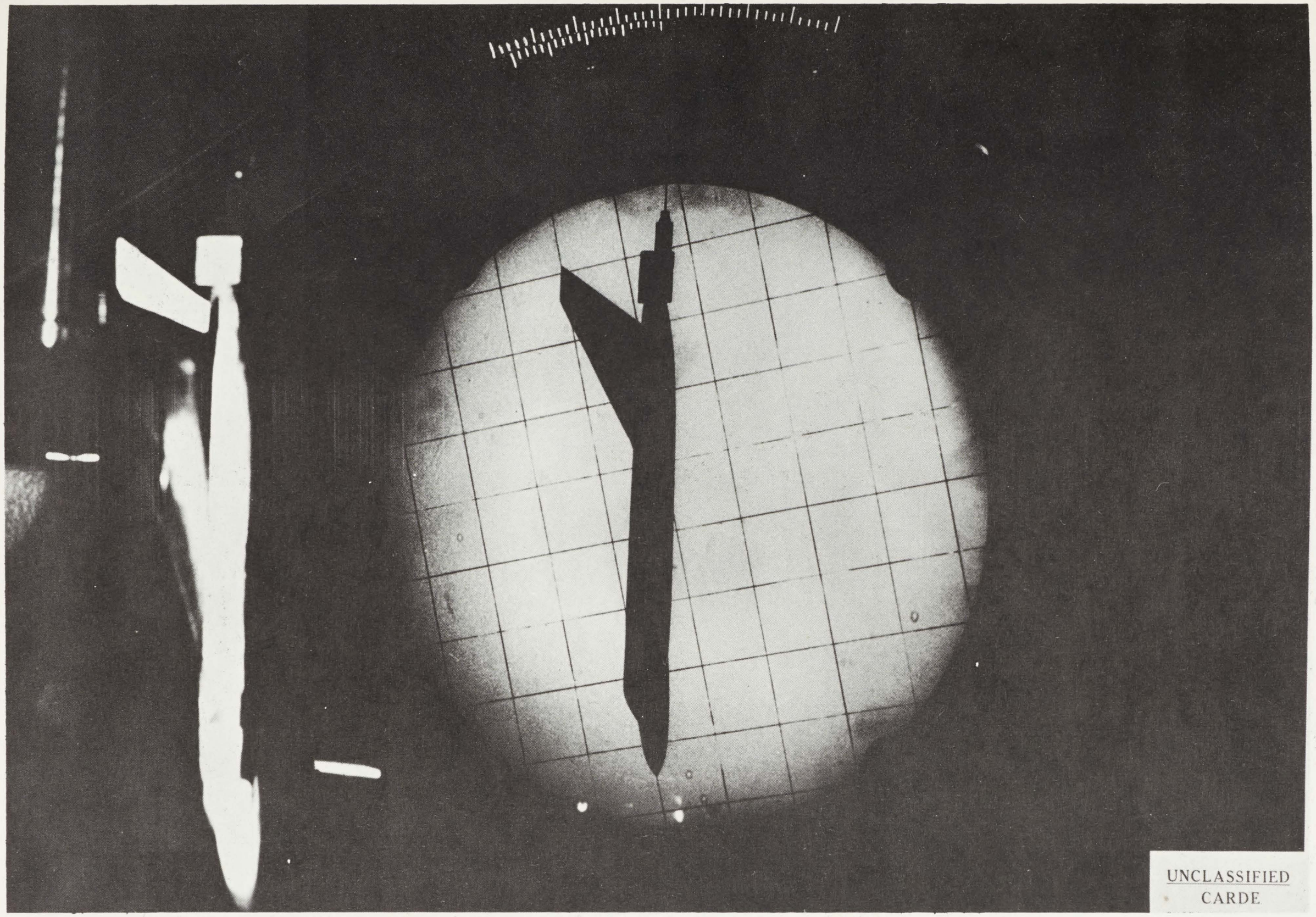

SHADOW METHOD. TORSIONAL PENDULUM

FIGURE 6

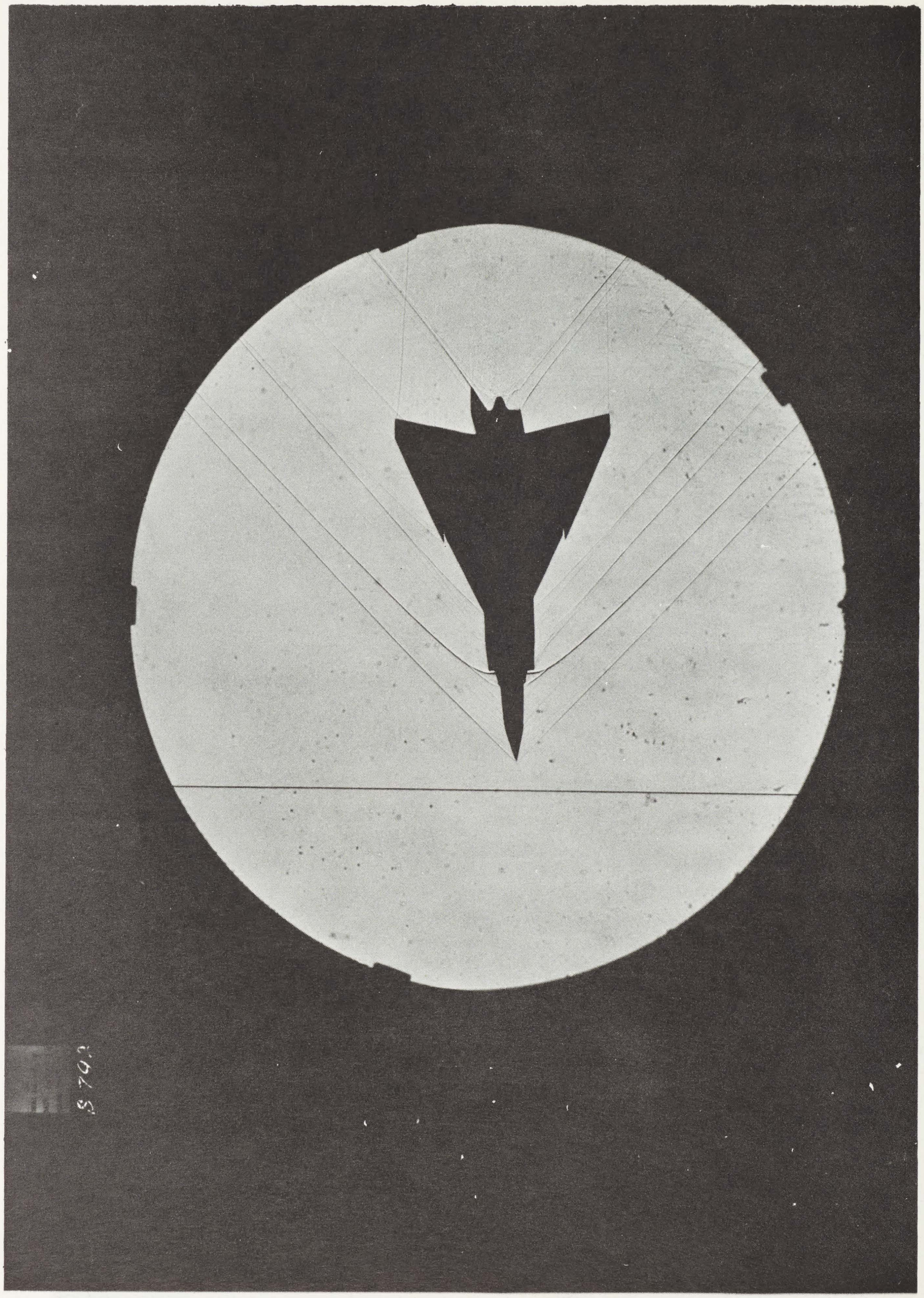

SHADOWGRAPH OF MODEL 10—19

FIGURE 7(a)

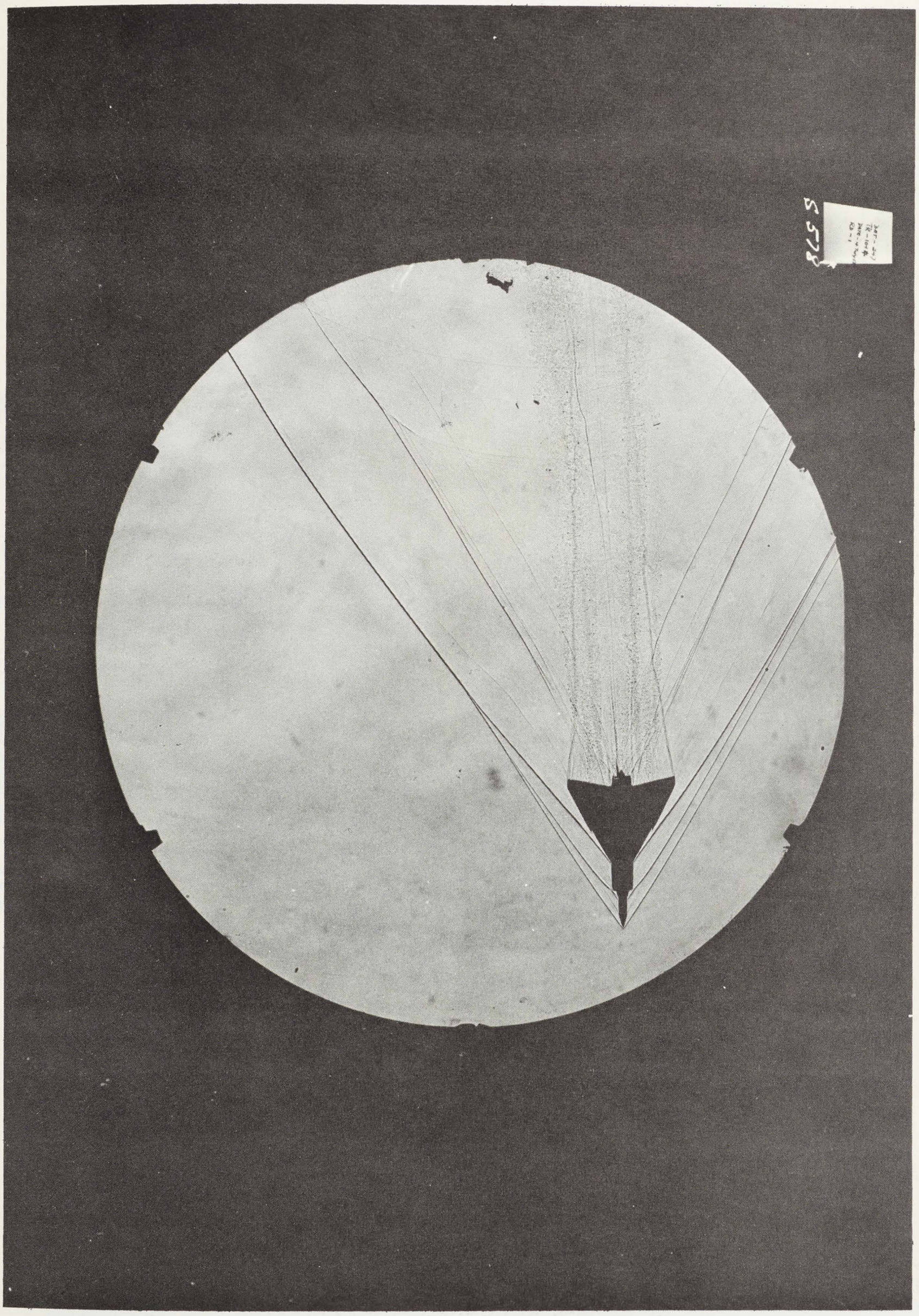

SHADOWGRAPH OF MODEL 10-14

FIGURE 7 (b)

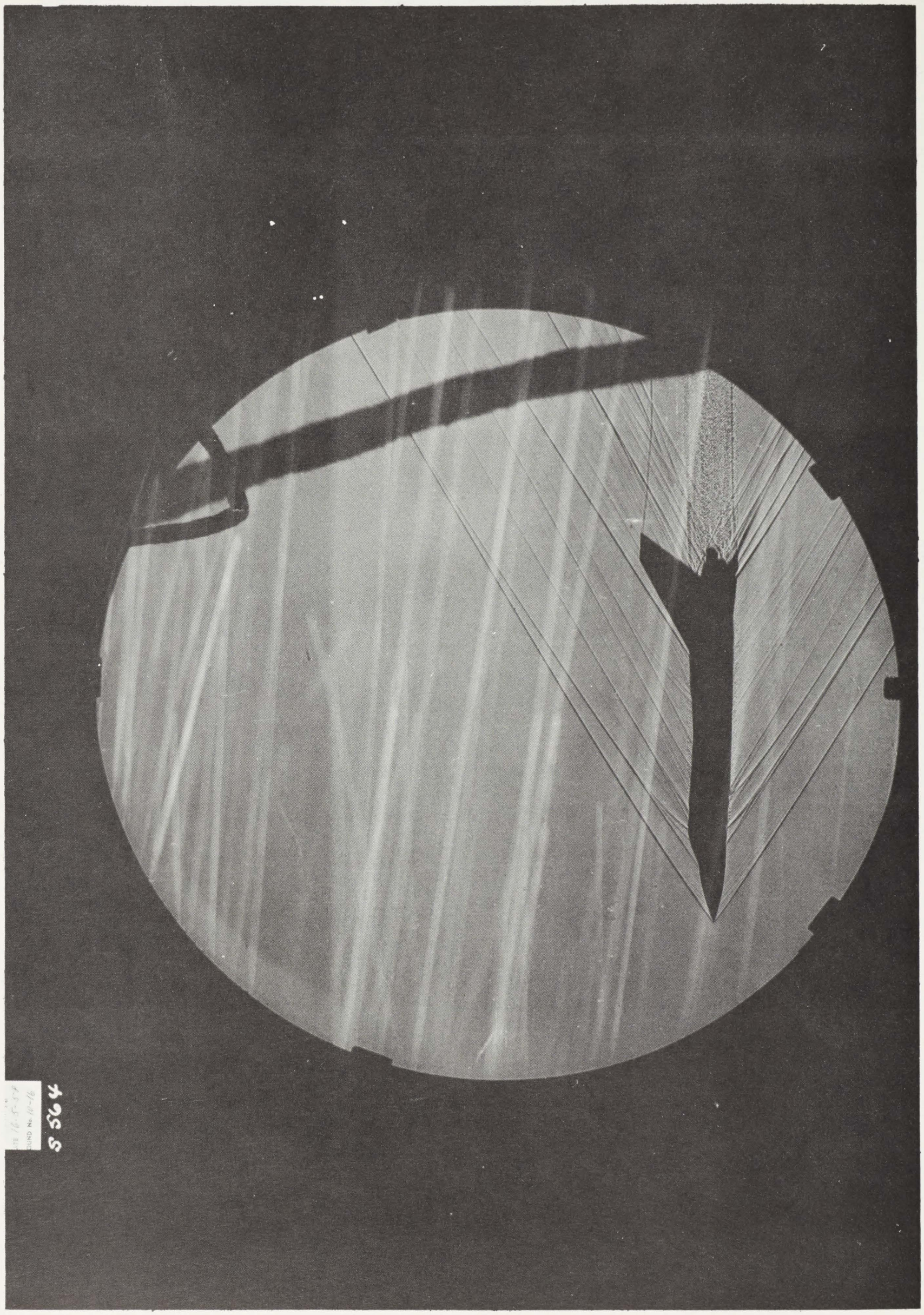

SHADOWGRAPH OF MODEL 10—16

FIGURE 7(c)

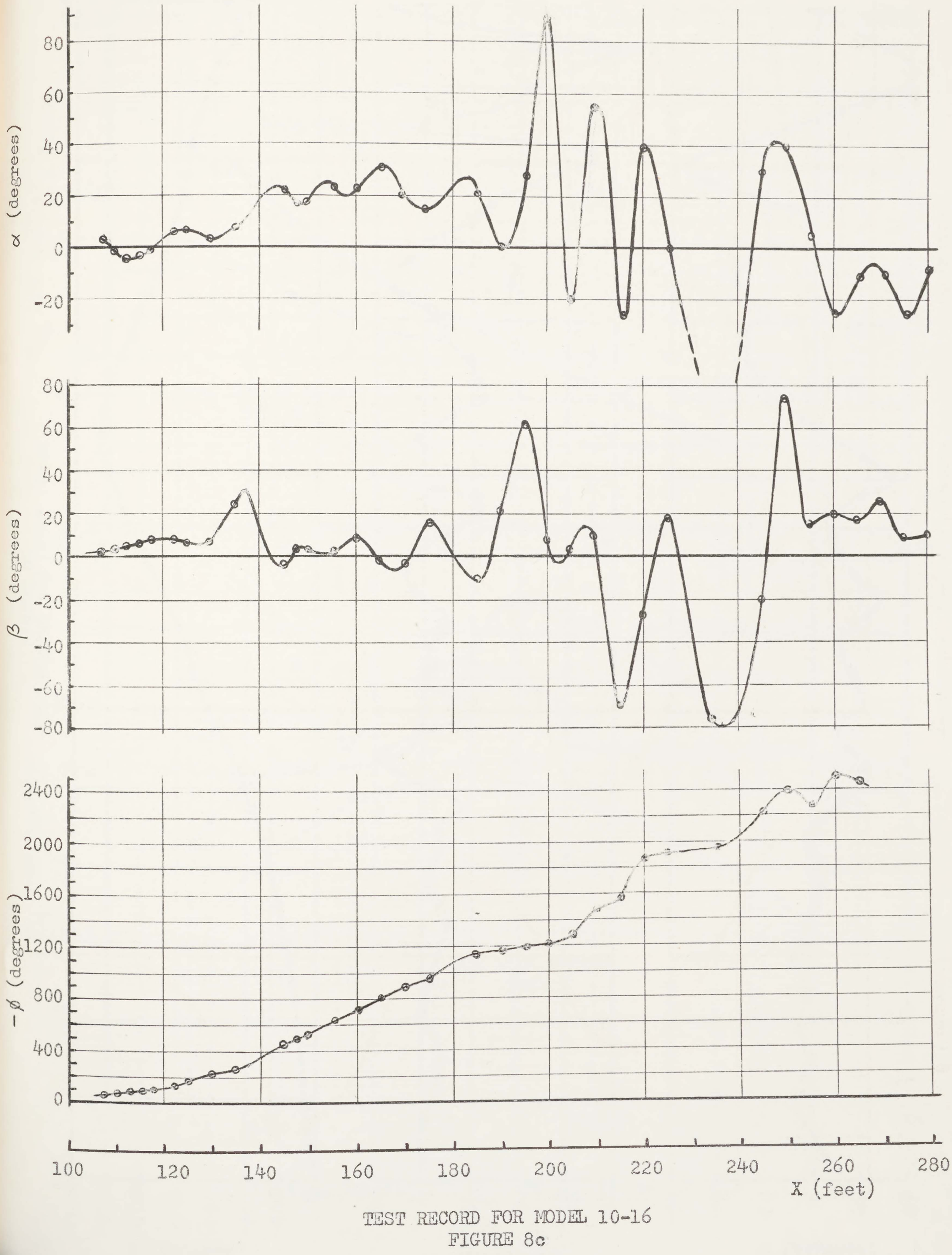

TEST RECORD FOR MODEL 10-16
FIGURE 8c

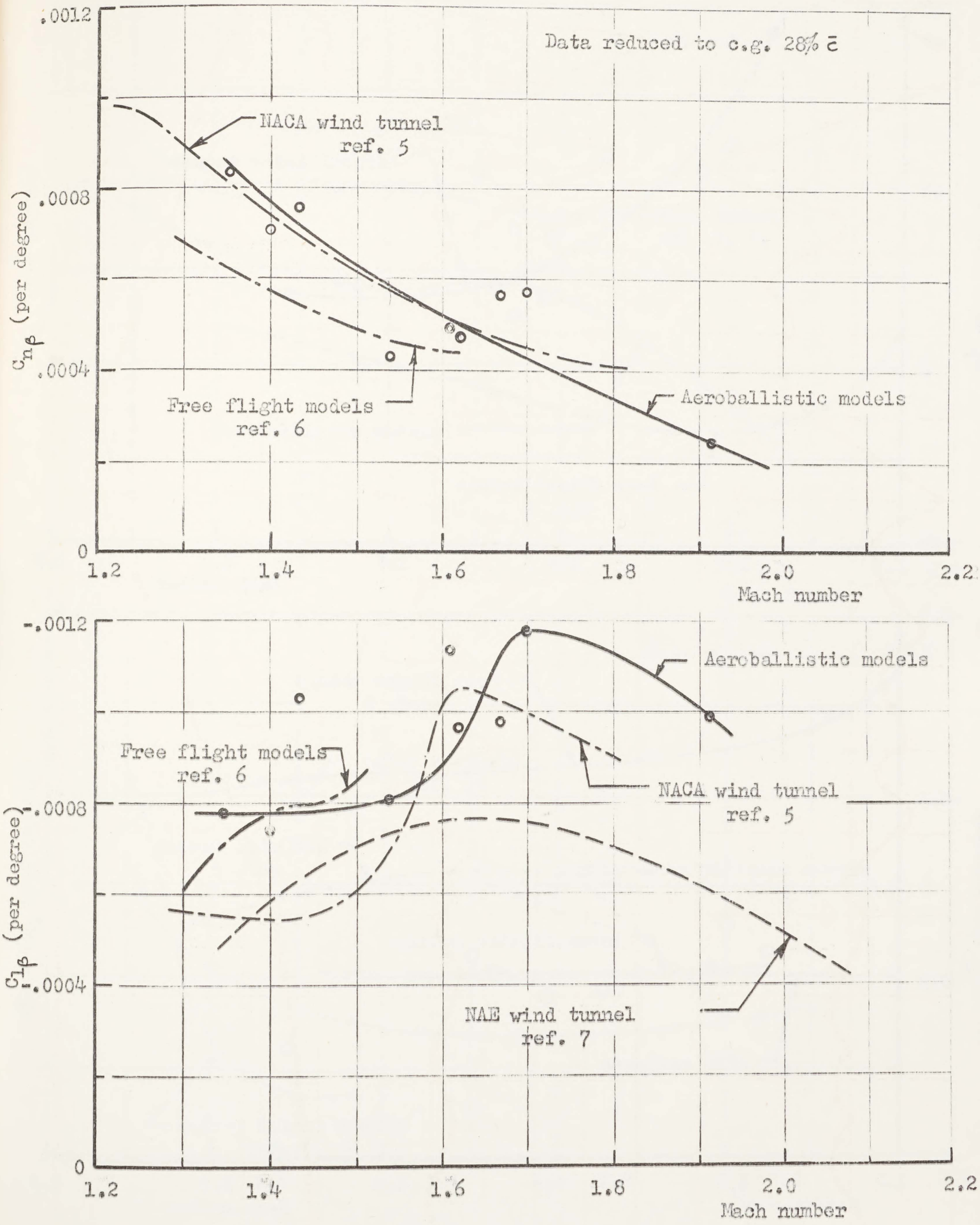

LATERAL DERIVATIVES C_{n_β} AND C_{l_β} VS. MACH NUMBER

FIGURE 9a

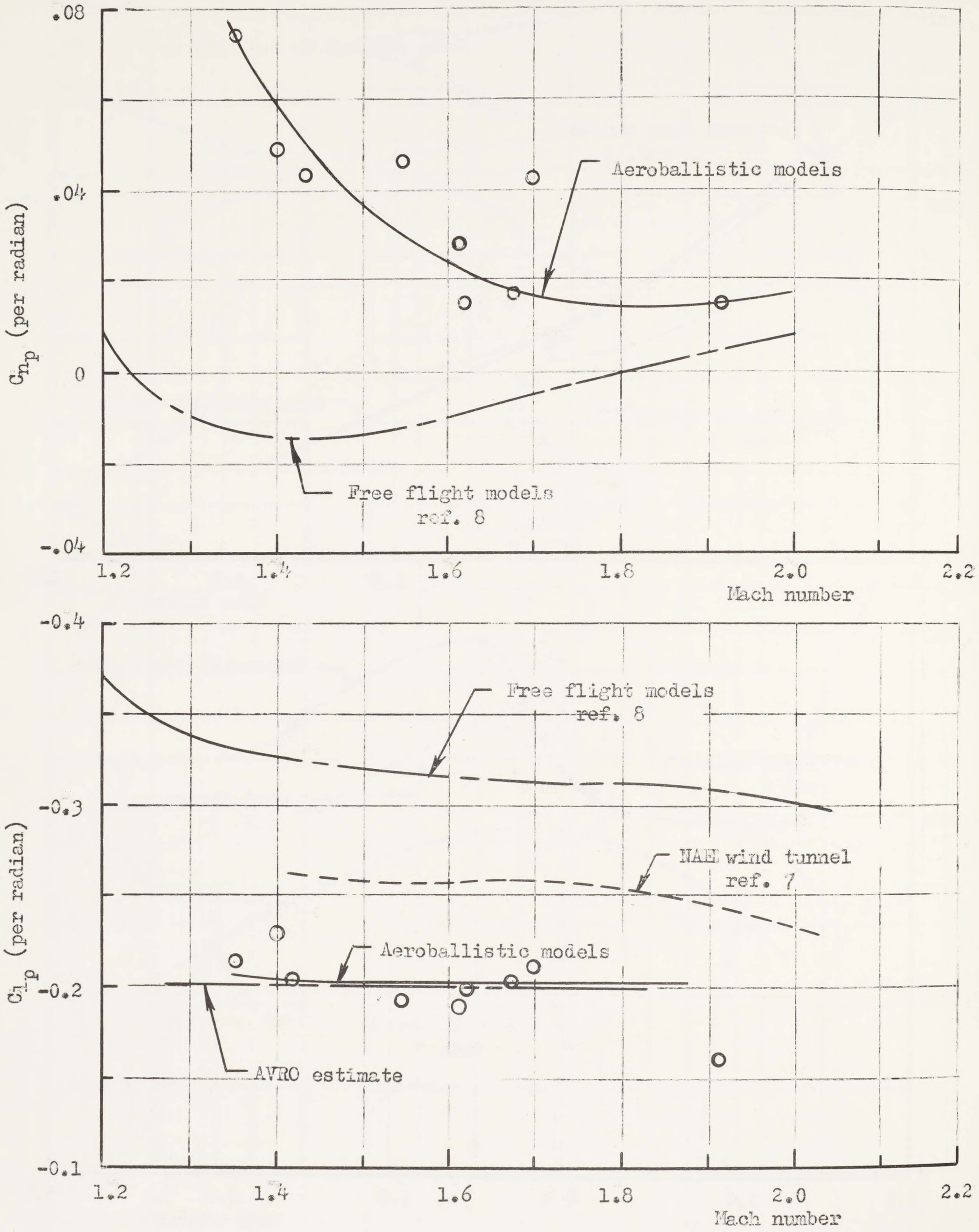

LATERAL DERIVATIVES C_{n_p} and C_{l_p} VS. MACH NUMBER

FIGURE 9b

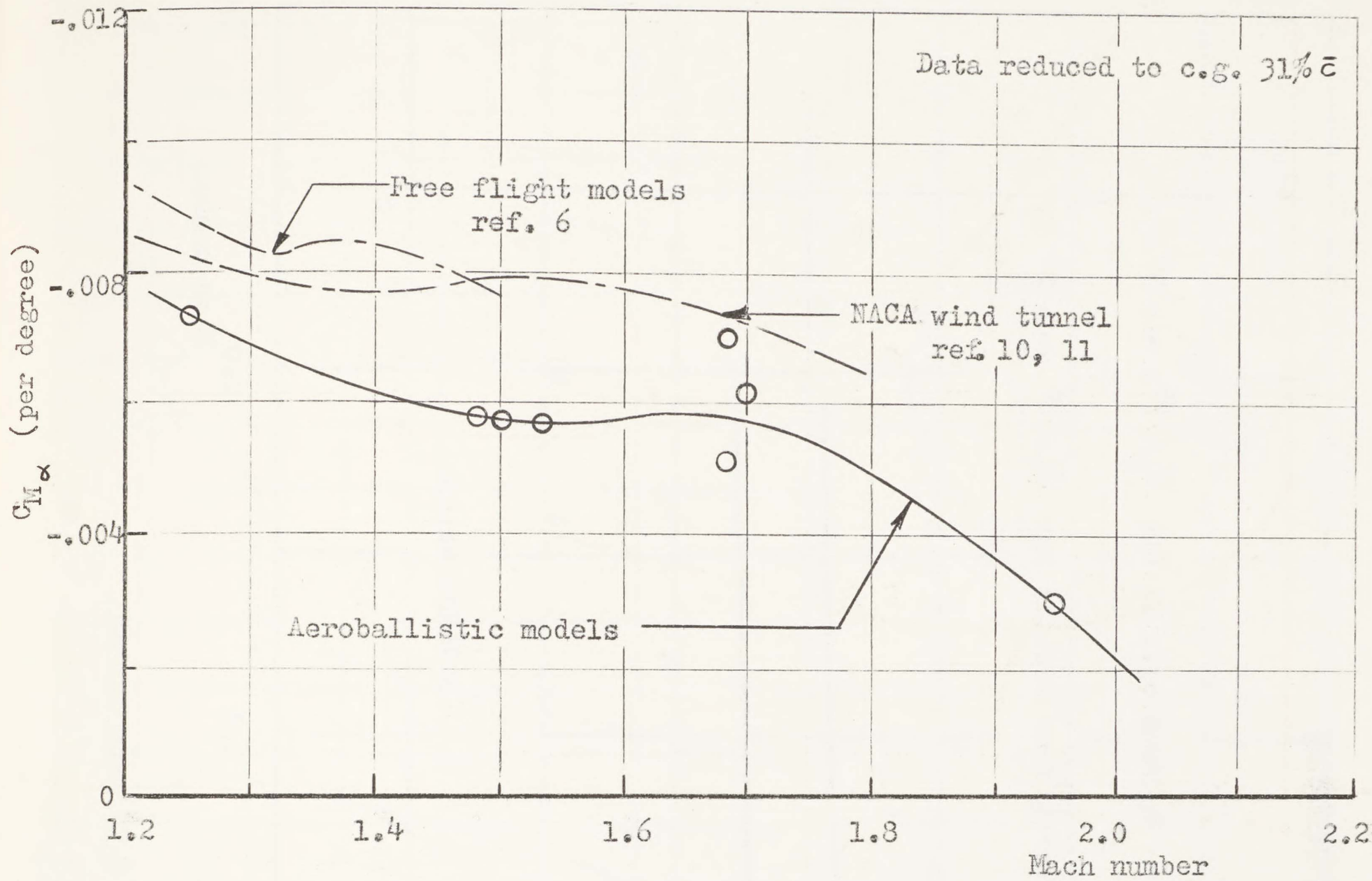

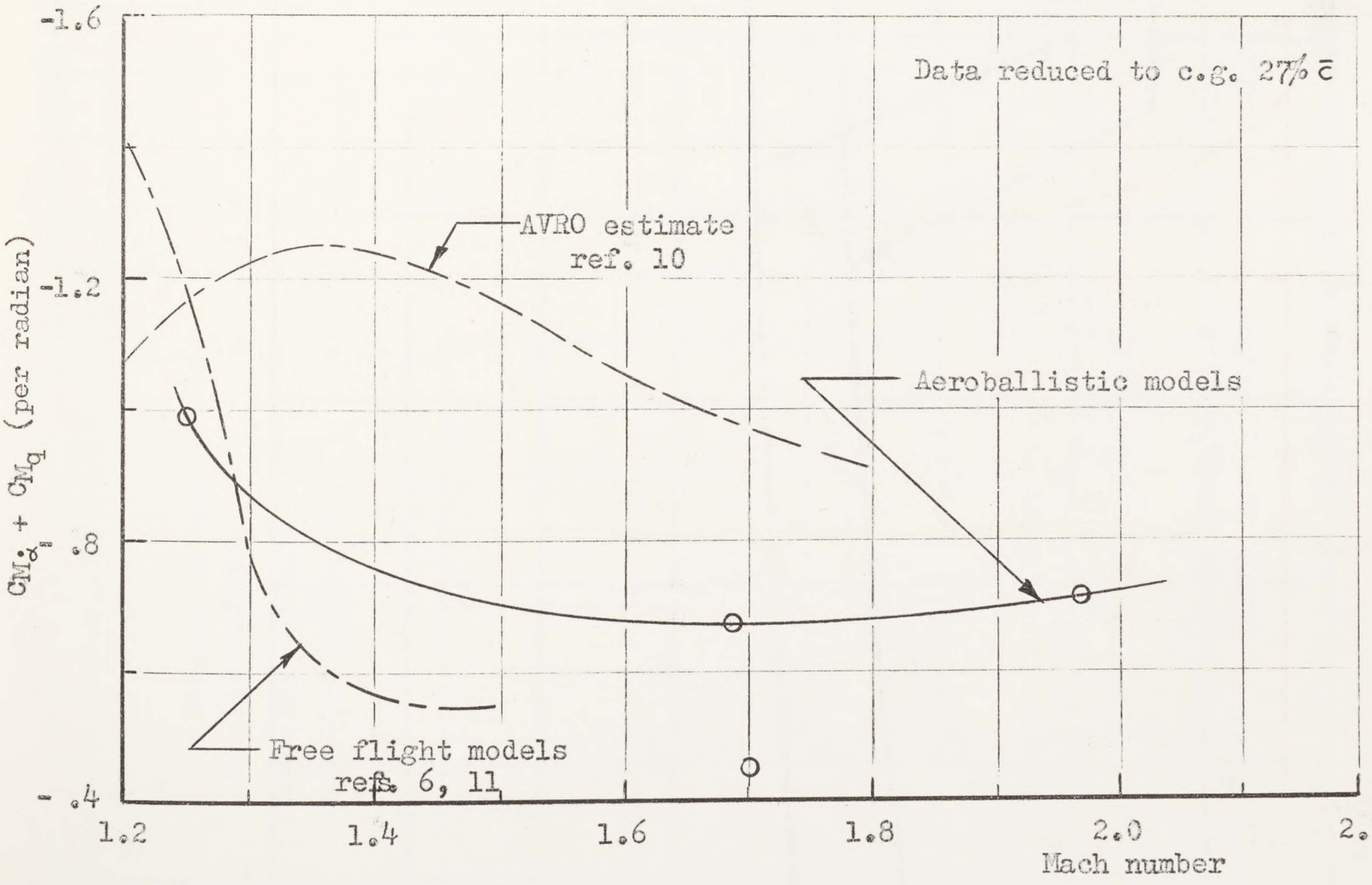

LONGITUDINAL DERIVATIVES C_{M_α} AND $(C_{M_{\dot\alpha}} + C_{M_q})$ VS. MACH NUMBER

FIGURE 10

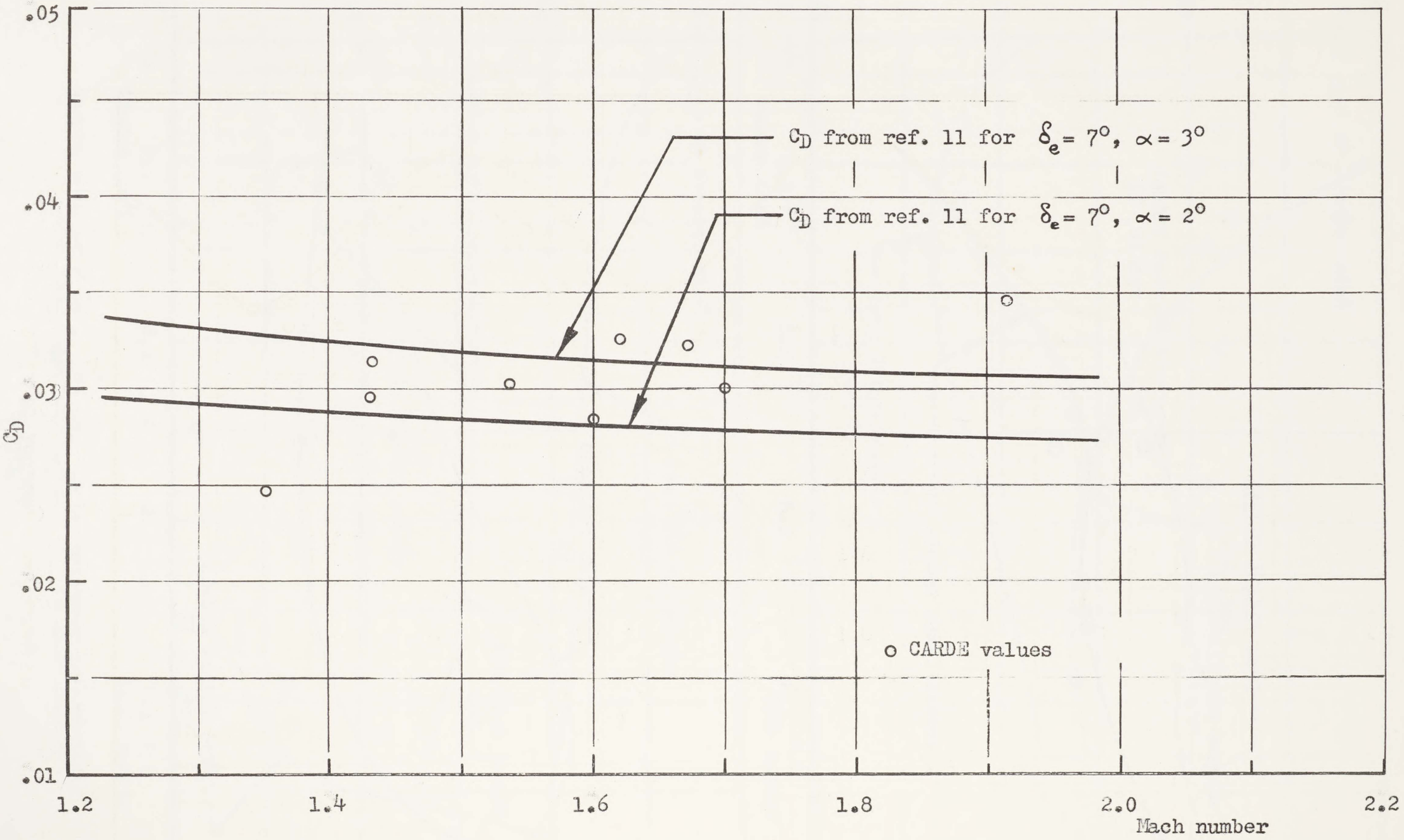

TOTAL DRAG COEFFICIENT C_D VS. MACH NUMBER

FIGURE 11

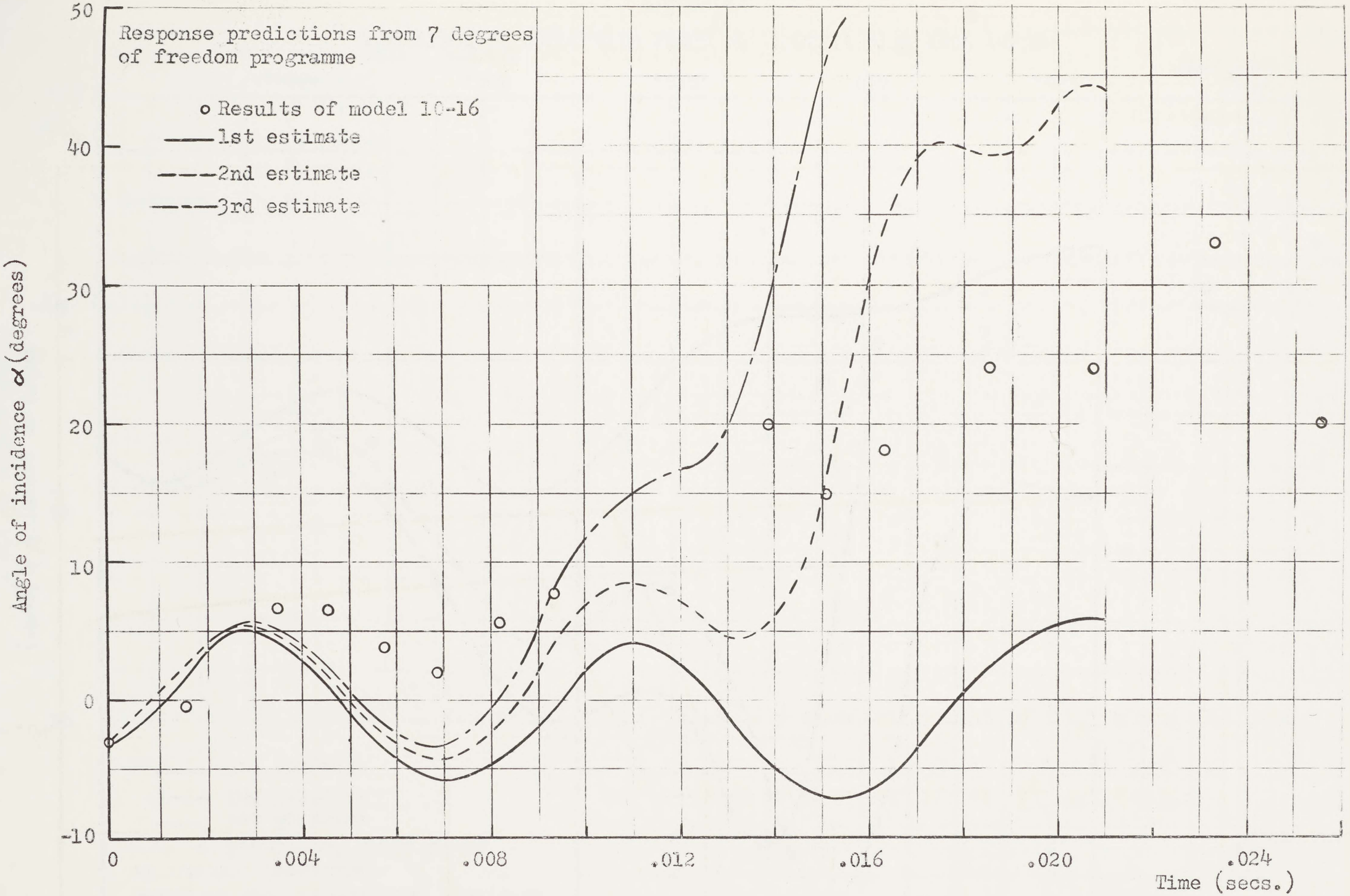

COMPARISON OF CALCULATED ANGLE OF ATTACK WITH TEST VALUES

FIGURE 12

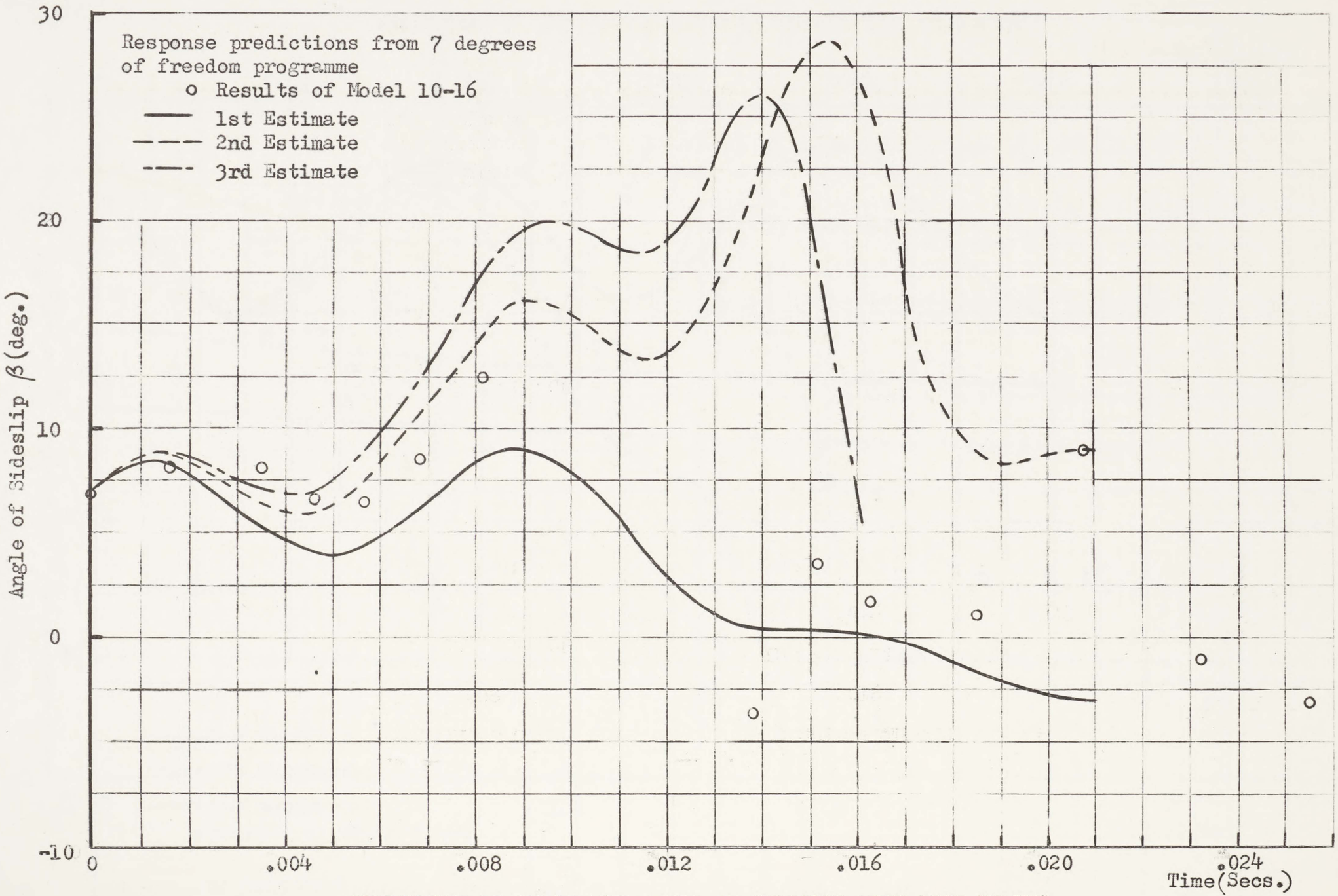

COMPARISON OF CALCULATED ANGLE OF SIDESLIP WITH TEST VALUES

FIGURE 13

FIGURE 13

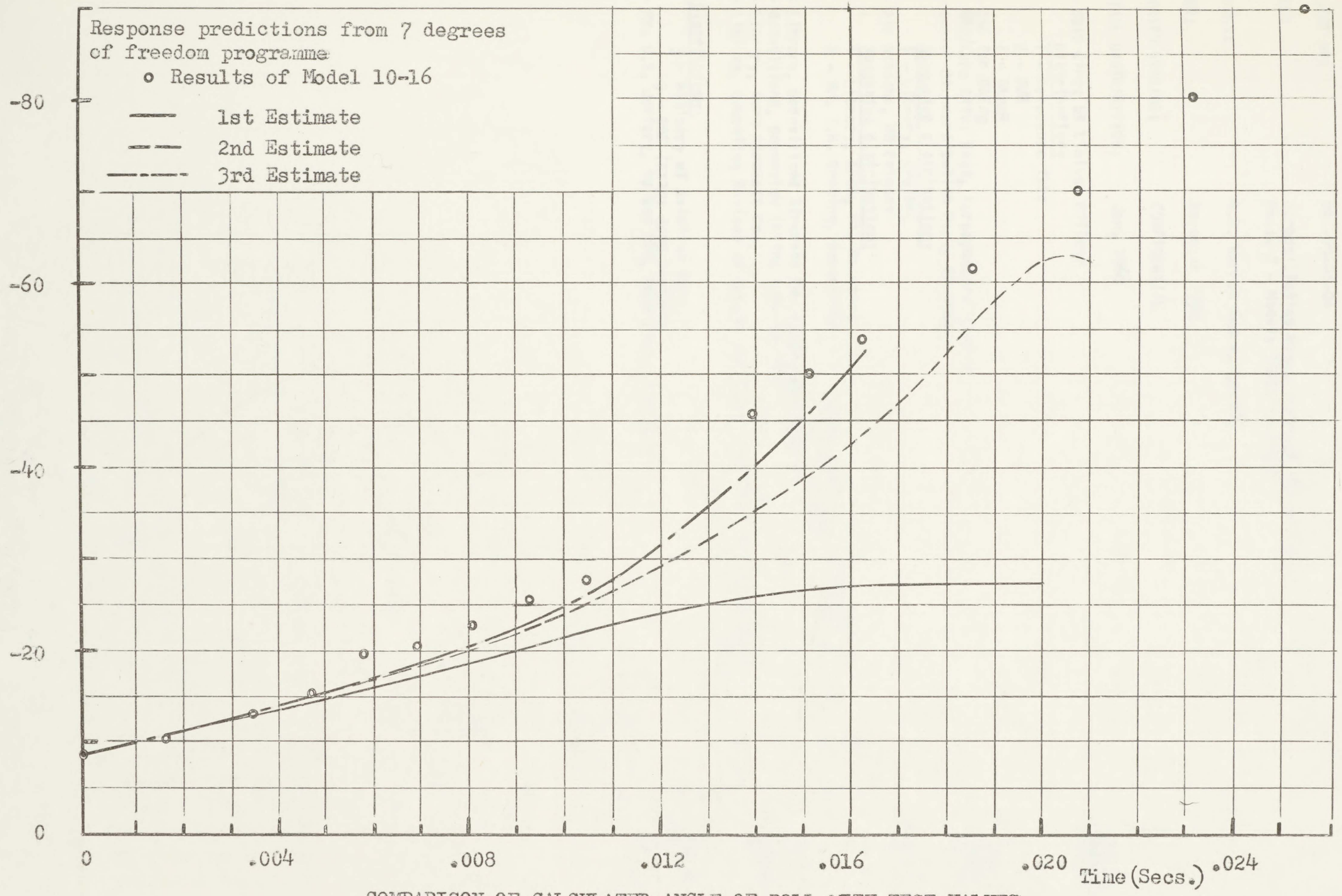

COMPARISON OF CALCULATED ANGLE OF ROLL WITH TEST VALUES

FIGURE 14

REPORT: CARDE Technical Memorandum AB-46

PROJECT NO: 04[illegible]-03-01-04

TITLE: Aeroballistics Range Tests of the CF-105
Phase 2 - Models 10-11 to 10-25

AUTHORS: H.R. Warren and B. Cheers

DATED: November 1959

SECURITY GRADING: CONFIDENTIAL

INITIAL DISTRIBUTION: Jan. 1960

Copy Nos.

5 - DSIS Circ: UK Liaison Officer — 15-19
Distribution:
1 - Reference file
2 - DWR
1 - DEngR
2 - CAE for DAEng — 20-21
2- NRC/Aero Attn: Head, Aerodynamics Section — 22-23
1 - Senior Standardization Rep., US Army — 24
Suggested distribution:
1 - Library, APG/BRL
2 - Air Attache, US Embassy — 25-26
Suggested distribution:
1 - Library, ARDE, Ft. Halstead
1 - Mr. T.N. Canning, Supersonic Free Flight, Ames Research Center, N.A.S.A., Moffett Field, California
1 - Library, DeHavilland Aircraft Co. (Attn: GM Division) — 27
1 - DeHavilland, Downsview (Attn: H.R. Warren) — 28
2 - Library, Avro Aircraft Co., — 29-30
1 - Library, Computing Devices of Canada Ltd. (Attn: Technical Services Branch) — 31

UK Distribution:
3 - Ministry of Aviation for: — 32-34
3 - RAE (Attn: Aero Section)
1 - Mr. C.B. Jeffery, PO Box 268, Cold Lake, Alberta — 35

CONFIDENTIAL